Received: 7 March 2022 | Accepted: 17 June 2022

DOI: 10.1002/hep4.2038

ORIGINAL ARTICLE

A missense mutation in the proprotein convertase gene *furinb* causes hepatic cystogenesis during liver development in zebrafish

Jillian L. Ellis[1] | **Kimberley J. Evason**[2,3] | **Changwen Zhang**[1] | **Makenzie N. Fourman**[1] | **Jiandong Liu**[2,4] | **Nikolay Ninov**[2,5,6] | **Marion Delous**[2,7] | **Benoit Vanhollebeke**[2,8] | **Ian Fiddes**[2] | **Jessica P. Otis**[9,10,11] | **Yariv Houvras**[12] | **Steven A. Farber**[9,10] | **Xiaolei Xu**[13] | **Xueying Lin**[13] | **Didier Y. R. Stainier**[2,14] | **Chunyue Yin**[1,2,15]

[1]Division of Gastroenterology, Hepatology, and Nutrition, Cincinnati Children's Hospital Medical Center, Cincinnati, Ohio, USA

[2]Department of Biochemistry and Biophysics, Program in Developmental and Stem Cell Biology, Liver Center and Diabetes Center, University of California, San Francisco, San Francisco, California, USA

[3]Huntsman Cancer Institute and Department of Pathology, University of Utah, Salt Lake City, Utah, USA

[4]McAllister Heart Institute, Department of Pathology and Laboratory Medicine, School of Medicine, The University of North Carolina at Chapel Hill, Chapel Hill, North Carolina, USA

[5]Center for Regenerative Therapies TU Dresden, Dresden, Germany

[6]Paul Langerhans Institute Dresden of the Helmholtz Center Munich at the University Hospital Carl Gustav Carus of TU Dresden, German Center for Diabetes Research, Dresden, Germany

[7]Equipe GENDEV, Centre de Recherche en Neurosciences de Lyon, Inserm U1028, CNRS UMR5292, Universite Lyon 1, Universite St Etienne, Lyon, France

[8]Laboratory of Neurovascular Signaling, Department of Molecular Biology, ULB Neuroscience Institute, Universite Libre de Bruxelles, Gosselies, Belgium

[9]Department of Embryology, Carnegie Institution for Science, Baltimore, Maryland, USA

[10]Department of Biology, Johns Hopkins University, Baltimore, Maryland, USA

[11]Department of Molecular and Cellular Biology and Biochemistry, Brown University, Providence, Rhode Island, USA

[12]Weill Cornell Medical College and New York Presbyterian Hospital, New York, New York, USA

[13]Department of Biochemistry and Molecular Biology, Department of Cardiovascular Medicine, Mayo Clinic, Rochester, Minnesota, USA

[14]Department of Developmental Genetics, Max Planck Institute for Heart and Lung Research, Bad Nauheim, Germany

[15]Division of Developmental Biology, Cincinnati Children's Hospital Medical Center, Cincinnati, Ohio, USA

Correspondence
Chunyue Yin, Division of Gastroenterology, Hepatology and Nutrition, Cincinnati Children's Hospital Medical Center, 3333 Burnet Ave., Cincinnati, OH 45229, USA.
Email: chunyue.yin@cchmc.org

Funding information
Cincinnati Children's Research Foundation, Grant/Award Number: Arnold W. Strauss Fellow Award, Trustee Award and the Peter and Tommy Colucci Research Award for PFIC; Damon Runyon Cancer Research Foundation, Grant/Award Number: DRG-109-10; Liver Center, University of California, San Francisco, Grant/Award Number:

Abstract

Hepatic cysts are fluid-filled lesions in the liver that are estimated to occur in 5% of the population. They may cause hepatomegaly and abdominal pain. Progression to secondary fibrosis, cirrhosis, or cholangiocarcinoma can lead to morbidity and mortality. Previous studies of patients and rodent models have associated hepatic cyst formation with increased proliferation and fluid secretion in cholangiocytes, which are partially due to impaired primary cilia. Congenital hepatic cysts are thought to originate from faulty bile duct development, but the underlying mechanisms are not fully understood. In a forward genetic screen, we identified a zebrafish mutant that developed hepatic cysts

Pilot/Feasibility grant; National Cancer Institute, Grant/Award Number: K08 CA172288 and R01 CA222570; National Institute of Diabetes and Digestive and Kidney Diseases, Grant/Award Number: P30 DK078392 and R01 DK117266-01A1; National Institute on Alcohol Abuse and Alcoholism, Grant/Award Number: R00 AA020514

during larval stages. The cyst formation was not due to changes in biliary cell proliferation, bile secretion, or impairment of primary cilia. Instead, time-lapse live imaging data showed that the mutant biliary cells failed to form interconnecting bile ducts because of defects in motility and protrusive activity. Accordingly, immunostaining revealed a disorganized actin and microtubule cytoskeleton in the mutant biliary cells. By whole-genome sequencing, we determined that the cystic phenotype in the mutant was caused by a missense mutation in the *furinb* gene, which encodes a proprotein convertase. The mutation altered Furinb localization and caused endoplasmic reticulum (ER) stress. The cystic phenotype could be suppressed by treatment with the ER stress inhibitor 4-phenylbutyric acid and exacerbated by treatment with the ER stress inducer tunicamycin. The mutant liver also exhibited increased mammalian target of rapamycin (mTOR) signaling. Treatment with mTOR inhibitors halted cyst formation at least partially through reducing ER stress. *Conclusion*: Our study has established a vertebrate model for studying hepatic cystogenesis and illustrated the contribution of ER stress in the disease pathogenesis.

INTRODUCTION

Cystic hepatic lesions, which are characterized by progressive formation of multiple fluid-filled cysts throughout the liver, affect up to 15%–18% of the population in the United States.[1] Some patients develop hepatomegaly that compresses neighboring organs and causes discomfort. Cyst hemorrhage, infection or rupture, and progression to secondary fibrosis, cirrhosis, or cholangiocarcinoma may lead to significant morbidity and mortality.[1] Traditional treatment for symptomatic hepatic cysts includes physical removal or emptying of cysts.[2] Somatostatin analogues are used to treat patients with severe disease, but the treatment is chronic, costly, and the benefits are modest.[3] Liver transplantation remains the only definitive treatment.[2]

Cyst formation has been associated with cellular defects within the cholangiocytes, including hyperproliferation, enhanced fluid secretion, changes in matrix-cell interactions, and disruption in cell adhesion and polarity (reviewed by Fabris et al.[4]). Meanwhile, congenital hepatic cysts that initiate in the fetal liver may result from faulty biliary development independent of cholangiocyte hyperproliferation.[5,6] Cholangiocytes possess primary cilia that serve as mechanosensors, osmosensors, and chemosensors.[7] Malformation and dysfunction of primary cilia result in cholangiocyte hyperproliferation and alter their fluid secretion and bile absorption, all of which contribute to cyst formation and growth. Genetic studies have linked mutations in ciliary genes to inherited polycystic liver disease (PLD). Mutations in *PKD1* and *PKD2*, which encode the ciliary-associated proteins polycystin-1 (PC1) and PC2, respectively, cause autosomal dominant polycystic kidney disease (ADPKD) that often manifests with liver cysts.[8,9] Mutations in *PKHD1*, which encodes a primary cilium protein fibrocystin, are associated with autosomal recessive polycystic kidney disease (ARPKD).[10] Isolated polycystic liver diseases have been linked to mutations in genes including Protein kinase C substrate 80K-H (*PRKCSH*), SEC63 homolog, protein translocation regulator (*SEC63*), LDL receptor related protein 5 (*LRP5*), SEC61 translocon subunit beta (*SEC61B*), ALG8 α-1,3-glucosyltransferase (*ALG8*), Glucosidase II α subunit (*GANAB*), and ALG9 α-1,2-mannosyltransferase (*ALG9*) (reviewed by Masyuk et al.[11]). Except for *LRP5*, all of these genes encode proteins located in the endoplasmic reticulum (ER). Mutations in the known disease genes account for only 50% of clinical cases of PLD,[4] leaving the door open for finding additional genes and mechanisms in hepatic cystogenesis.

Zebrafish have been used to study biliary development and disease, including PLD.[12] Zebrafish injected with morpholinos targeting *sec63*, *prkcsh*, and polycystic kidney disease 1a (*pkd1a*) exhibit ultrastructural features of hepatic cyst formation.[13] *sec63* mutants have excessive ER stress in the liver.[14] However, no genetic mutant with hepatic cysts has been reported in zebrafish.

In a forward genetic screen, we identified a zebrafish mutant that develops hepatic cysts at larval stages. Hepatic cystogenesis in the mutant is not driven by cholangiocyte hyperproliferation or defects in the primary cilium, but rather by failure to make interconnecting bile ducts during liver development. We determined that a missense mutation in the *furinb*

gene, which encodes a proprotein convertase, is responsible for the biliary phenotypes. The mutation leads to mislocalization of Furinb and ER stress. Treatment with ER stress inhibitor or mammalian target of rapamycin (mTOR) inhibitors partially suppressed cyst formation in the mutants.

EXPERIMENTAL PROCEDURES

Zebrafish

Wild-type (WT), *furinb*$^{s741+/-}$, *furinb*$^{ci204+/-}$, *muc2.2*$^{ci205+/-}$, *pkd1a*$^{zf1067+/-}$, *pkd1b*$^{zf1070+/-}$,[15] *Tg(EPV.Tp1-Mmu.Hbb:EGFP)*^{um14}*/Tg(Tp1:GFP)*, *Tg(EPV.Tp1-Mmu.Hbb:hist2h2l-mCherry)*^{s939}*/Tg(Tp1:H2B-mCherry)*,[16] *Tg(mpeg1:YFP)*^{w200Tg}, and *Tg(EPV.Tp1-Mmu.Hbb:mCherry-CAAX)*^{s733}*/Tg(Tp1:ras-mCherry)* zebrafish were raised and maintained under standard laboratory conditions in accordance with the Guide for the Care and Use of Laboratory Animals (National Institutes of Health publication 86–23, revised 1985) and approved by the Institutional Animal Care and Use Committee at the Cincinnati Children's Hospital Medical Center. Animals of both genders were studied.

Whole-genome sequencing and genotyping

Whole-genome sequencing was conducted at the University of California, San Francisco Genomics Core as described.[17] Sequencing was performed on pools of 50 *s741* mutants and 50 phenotypically WT siblings based on the bile duct phenotypes, as revealed by *Tg(Tp1:GFP)* transgene expression. Genomic DNA was prepared using the DNeasy blood and tissue kit (Qiagen) and sequenced on the Illumina HiSeq 2000. Data were analyzed using SNPtrack (http://genetics.bwh.harvard.edu/snptrack/). *s741* mutation was genotyped by polymerase chain reaction (PCR) on genomic DNAs using the following primers: forward 5′-TTCTGTCGGAGGACCAAACT −3′ and reverse 5′-ACACACACACACCCACTGGT −3′. The 499 bp PCR product was cut with restriction enzyme Bsp1286I (New England BioLabs). The mutant product was cut into 211 bp and 288 bp fragments, while the WT product remained uncut at 499 bp.

Immunofluorescence

Immunofluorescence staining on whole-mount larvae and 150-μm vibratome sections was performed as described.[18] Primary and secondary antibodies are listed in Table S1. The samples were imaged on a Nikon A1Rsi inverted confocal microscope (Nikon Instruments). Imaging processing and quantification were conducted using Imaris software (Bitplane).

BODIPY feeding assay

At 121 h post fertilization (hpf), WT and *s741* mutant larvae were incubated with 6.4 μmol/L BODIPY FL C_5 (Invitrogen) for 7 h as described.[12] Animals were imaged live on a confocal microscope to assess fluorescence in the gallbladder and liver.

Time-lapse live imaging

At 80 hpf, three WT and three *s741* mutant larvae expressing *Tg(Tp1:*GFP) were mounted in 1% low-melting agarose in a customized imaging chamber filled with 80 ml egg water containing 0.01% Tricaine (Sigma Aldrich). The chamber was maintained at 28°C for the duration of the time lapses. The 40-μm Z-stacks of epifluorescent images of the livers were collected at 8-min intervals for 14 h on a Nikon A1R Multiphoton upright confocal microscope using a ×20 water objective lens.

Genetic mosaic analysis by cell transplantation

Cell transplantation was performed at the blastoderm stage as described.[18] To target the donor cells to the endoderm, 200 pg of *casanova/sox32* messenger RNA (mRNA) was injected into the donor embryos at the one-cell stage. The donors were genotyped by PCR immediately following transplantation.

Chemical treatments

All the chemicals used in the drug treatment are listed in Table S2. The larvae expressing *Tg(Tp1:*GFP) were treated with 0.05% DMSO or various chemicals in egg water in the dark from 72 hpf to 120 hpf. Their genotypes were determined by PCR.

Furinb construct design and microinjection

To rescue *s741* phenotypes using WT *furinb* mRNA, a full-length *furinb* complementary DNA (cDNA) was amplified by PCR from WT total cDNA and inserted into the RNA synthesis plasmid pCS2+. Sense RNA was synthesized using the Ambion mMessage mMachine T7 transcription kit (Invitrogen). A total of 20–50 pg of capped *furinb* RNA was injected into the yolk of embryos from *s741* heterozygotes incrosses at the 1–4

cell stage. The injected larvae were fixed in 4% paraformaldehyde at 96 hpf and genotyped by PCR.

The *Tg(Tp1:wt-furinb-EGFP)*, *Tg(Tp1:s741-furinb-EGFP)*, *Tg(fabp10a:wt-furinb-GFP)*, and *Tg(fabp10a:s741-furinb-EGFP)* transgenic constructs were generated using the multisite gateway-based Tol2kit.[19]

Statistical analysis

Two-tailed Student's *t* test and one-way analysis of variance with a Tukey's *post-hoc* test were performed using GraphPad Prism (GraphPad Software).

RESULTS

A forward genetic screen identifies a zebrafish mutant with hepatic nodules

To identify regulators of intrahepatic bile duct development, we carried out an N-ethyl-N-nitrosourea chemical mutagenesis screen using the *Tg(EPV.Tp1-Mmu.Hbb:EGFP)*^{um14}*/Tg(Tp1:GFP)* transgenic zebrafish that express green fluorescent protein (GFP) under the control of a Notch-responsive element. This transgene marks intrahepatic bile ducts and pancreatic ducts.[20,21] Of the 100 F2 families screened, we isolated two recessive mutations, with one causing ductopenia and the other forming biliary nodules. *s741* mutants exhibited pericardial edema and degenerative pharyngeal arches (Figure 1A), accompanied by 100% lethality by 1 week of age. In the liver, although the *Tg(Tp1:*GFP)+ biliary cells in WT larvae formed a rudimental intrahepatic biliary ductal network by 96 hpf (Figure 1B,D–F), the *s741* mutant biliary cells clustered in nodules (Figure 1C,G–J). Histological staining showed that the mutant livers displayed a disorganized architecture with variations in hepatocyte size and loss of the orderly arrangement of regularly spaced hepatocytes (Figure 1K–M). There were scattered round to ovoid cyst-like spaces in the mutant liver (Figure 1L,M, arrows).

The intrahepatic biliary cells in *s741* mutants form cysts that retained bile fluids

To examine the bile flow in *s741* mutants, we administered fluorescent lipid analog BODIPY-FL C5:0 from 120 hpf to 128 hpf (Figure 2A–F). BODIPY C5:0 is absorbed by the liver and secreted with bile salts by the hepatocytes, allowing real-time tracking of bile secretion and flow.[22] In WT, BODIPY fluorescence was detected within the intrahepatic bile ducts marked by *Tg(Tp1:*ras-mCherry) expression (Figure 2A,C). In contrast, BODIPY fluorescence was retained within the nodules lined by the biliary cells in the mutants (Figure 2B,D), indicating that these nodules are fluid-filled cysts. In WT, bile is transported through the network of intrahepatic bile ducts and drained into the gallbladder, as reflected by the strong fluorescence in the gallbladder (Figure 2E). While the gallbladder still formed in *s741* mutants (Figure 2H), it was not filled with BODIPY (Figure 2F), suggesting that bile fluids were retained in the liver. Outside of the liver, we found cysts in the mutant pancreas, but not in the pronephric ducts (Figure S1).

In zebrafish, hepatocytes excrete bile fluids into the bile ducts through bile canaliculi on the apical membrane.[12] At 120 hpf, the bile canaliculi in *s741* mutants were shorter and dilated compared with WT, as revealed by the expression of bile canalicular transporter BSEP (bile salt export pump) (Figure 2I,J). We performed transmission electron microscopy (TEM) on the WT and mutant livers at 96 hpf, before the initiation of bile excretion in zebrafish.[22] The WT bile canaliculus contained tightly packed actin microvilli (Figure 2K, asterisk). The actin microvilli in the mutant canaliculus were sparse and disorganized (Figure 2L, asterisk). These observations imply that bile canalicular development was impaired in *s741* mutants independent of bile flow, consistent with the notion that biliary and bile canalicular development is highly coordinated.[20]

A missense mutation in furinb is responsible for the mutant liver phenotype

To isolate the molecular lesion responsible for the *s741* mutant phenotype, we scanned the genome for linkage to the phenotype using bulk segregant analyses and mapped the mutation to linkage group 25. We then performed whole-genome sequencing analyses.[17] Log-likelihood analysis revealed a 1.4-Mb interval, and none of the SNPs identified within the interval resulted in the gain of a new stop codon. Homozygosity scoring analysis showed two peaks within this interval (Figure 3A). The first peak was located in an area where no sequence reads were returned for the mutant pool, suggestive of a deletion. The deletion covered the first 15 exons of the transcript ENSDART00000112246 that corresponds to the gene *mucin2.2/muc2.2*. The second peak was located near the transcript of the gene *furinb* and contained three non-synonymous single-nucleotide polymorphisms (SNPs). We generated cDNAs from 50 mutants and 50 phenotypically WT siblings, then amplified and sequenced the open reading frames of *muc2.2* and *furinb*. All of the mutants were homozygous for the deletion in *muc2.2* and one of the three non-synonymous SNPs in *furinb*, whereas the unaffected siblings were WT or heterozygous for these mutations (Figure 3B; data not shown). We also

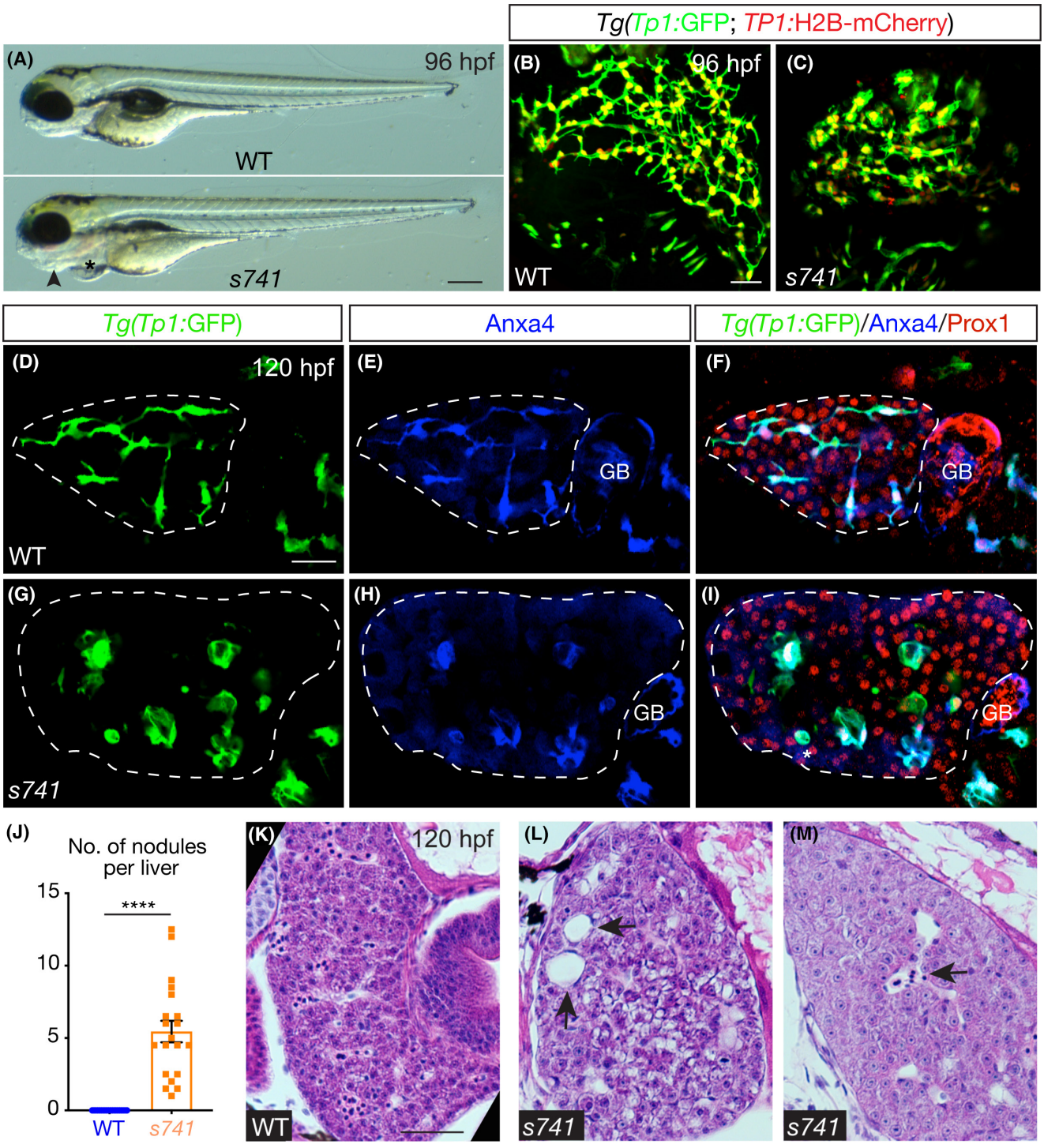

FIGURE 1 *s741* mutants develop hepatic nodules composed of intrahepatic biliary cells. (A) Live wild-type (WT; top) and *s741* mutant (bottom) larvae at 96 h pst fertilization (hpf). Lateral views; anterior is on the left. Arrowhead points to the degenerating pharyngeal arches and asterisk marks the pericardial edema. (B,C) Confocal three-dimensional (3D) projections of larvae expressing *Tg(Tp1:GFP* [green fluorescent protein]) (green) and *Tg(Tp1:H2B-mCherry)* (red) transgenes in the intrahepatic biliary cells. (D–I) Confocal single-plane images of the livers. (D,G) *Tg(Tp1:GFP)* transgene expression marks the intrahepatic biliary cells. (E,H) Annexin A4 (Anxa4) antibody stains the biliary cells.[50] (F,I) Merged images. Prox1 antibody labels the nuclei of hepatocytes and biliary cells. (B–I) Ventral views; anterior is to the top. (J) Numbers of *Tg(Tp1:*GFP)+ nodules (mean ± SEM) in the liver of WT (blue) and *s741* mutant (orange) larvae at 96 hpf. A nodule was defined as a cluster of two or more *Tg(Tp1:*GFP)+ cells that maintained one or no interconnecting ducts with other biliary cells. Each dot represents individual liver. Statistical significance was calculated by two-tailed Student's *t* test: ****$p < 0.0001$. (K–M) Hematoxylin and eosin stain of larval livers. Arrows in (L) point to cystic spaces that are entirely surrounded by hepatocytes and/or cholangiocytes. Arrow in (M) marks a cystic space that is lined by endothelium and contains red blood cells. Scale bars: 70 μm (A); 30 μm (B–I); and 50 μm (K–M). For experiments in (A)–(I) and (K)–(M), 10 WT and 10 mutants were examined and all of them exhibited the representative phenotypes. GB, gallbladder.

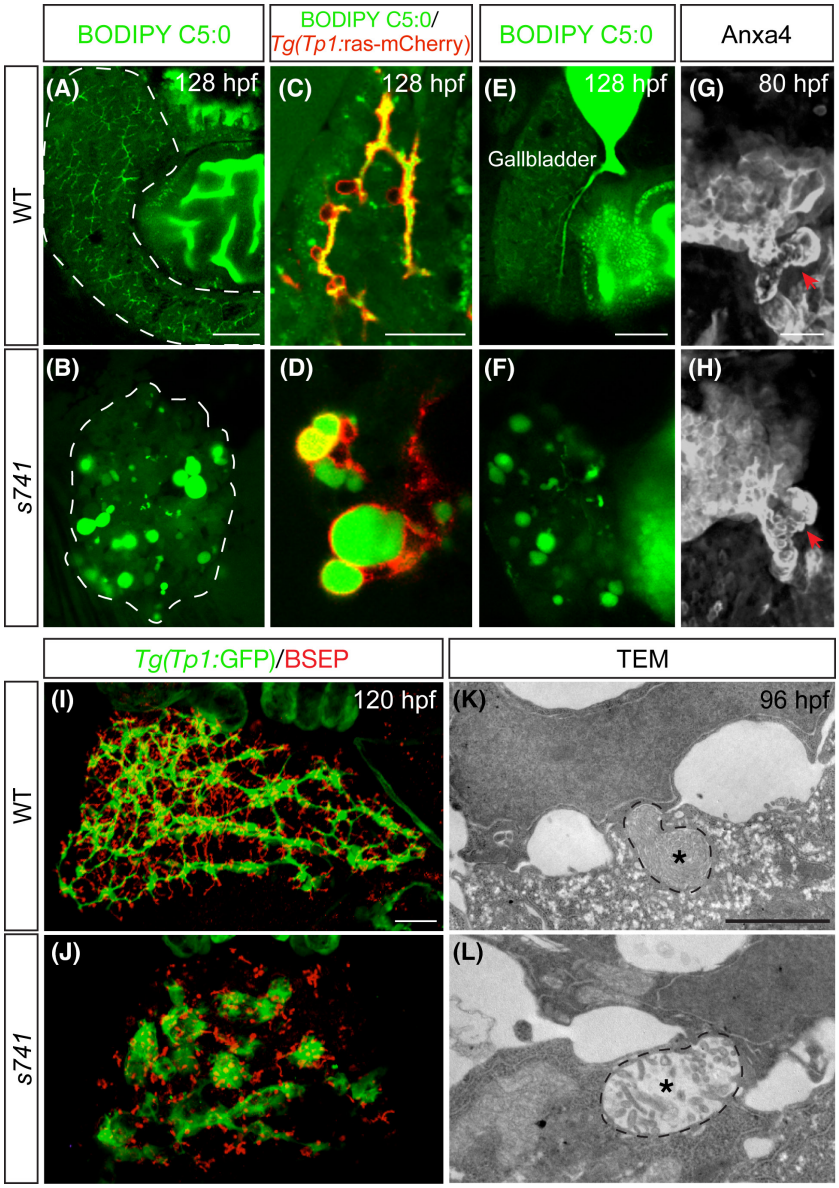

FIGURE 2 *s741* mutants form fluid-filled cysts in the liver. (A–F) Fluorescent micrographs of larval livers showing that the mutant liver retained BODIPY in the nodules. (C,D) Fluorescent micrograph images under higher magnification with *Tg(Tp1:*ras-mCherry) (red) transgene that marked the biliary cells. Twenty WT and 20 mutants were examined and all showed the representative phenotype. (G,H) Confocal 3D projections of the hepatopancreatic ductal system stained by Anxa4 antibody. Red arrows point to the gallbladder. (A–D,E–F) Lateral views taken from the left and right side of the fish, respectively. Anterior is on the left. (I,J) Confocal 3D projections showing the biliary cells marked by *Tg(Tp1:*GFP) expression (green) and bile canaliculi stained by bile salt export pump (BSEP) antibody. (G–J) Ventral views; anterior is on the top. Ten WT and 10 mutants were examined and all showed the representative phenotypes. (K,L) Representative transmission electron microscopy (TEM) images of the bile canaliculi (outlined by dashed line) at 96 hpf. Asterisks point to actin microvilli within the bile canaliculi. Six WT and 6 mutants were examined. Scale bars: 50 μm (A,B,E,F); 30 μm (C,D,G–J); and 2 μm (K,L).

sequenced the open reading frames of an additional 18 genes within the interval. There was no correlation between the presence of the non-synonymous or splice variants in these genes and the mutant phenotypes (data not shown).

To determine which mutation was responsible for the cystic phenotype in *s741* mutants, we first performed reverse-transcription PCR and found that *muc2.2* expression was absent in the livers of WT or *s741* mutant larvae at 96 hpf (Figure S2A). We generated a *muc2.2* mutant allele that resembles the deletion found in *s741* mutants by CRISPR/Cas9 genome editing (Figure S2B). The mutants did not have obvious bile duct phenotypes at 96 hpf (Figure S2C,D). These two results implicate that the *muc2.2* mutation unlikely accounts for the *s741* mutant phenotypes.

furinb is one of the zebrafish orthologs of the mammalian *Furin* gene that encodes an endoprotease belonging to a family of proprotein convertases.[23] The missense mutation found in *s741* mutants causes a

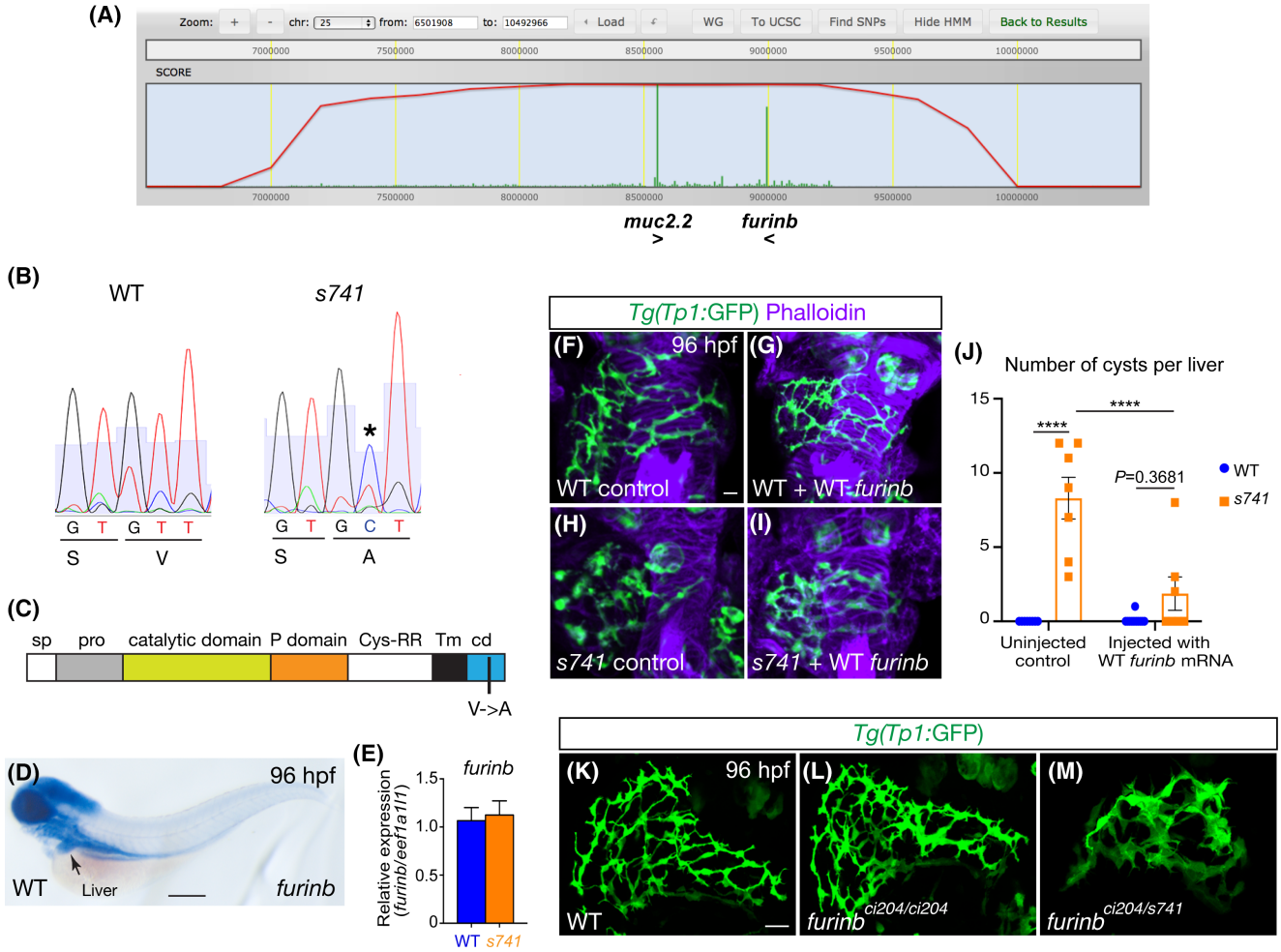

FIGURE 3 A missense mutation in the *furinb* gene is responsible for the cystic phenotype in *s741* mutants. (A) Genome view of linkage analysis using SNPtrack. Log likelihood analysis (red line) returned an approximate 1.4-Mb interval on linkage group 25 for the presumptive mutation. The homozygosity score (green) suggested two candidate mutations in the *muc2.2* and *furinb* genes. (B) Sequencing of complementary DNA from *s741* mutants and WT siblings. Mutants bear a T-to-C mutation (indicated by *) near the C terminus, leading to a V-to-A amino acid change. (C) Domain diagram of Furinb protein. The V-to-A change occurs within the cytoplasmic domain (cd). (D) Whole-mount *in situ* hybridization detecting *furinb* transcript in WT at 96 hpf. Lateral view; anterior is on the left. (E) Quantitative polymerase chain reaction (PCR) analysis comparing *furinb* transcripts in the WT and *s741* mutant larval livers at 96 hpf. Triplicates were performed. The results are represented as relative expression levels normalized to the housekeeping gene *eef1a1l1* (mean ± SEM). Statistical significance was calculated by two-tailed Student's *t* test: $p = 0.7877$. (F–I) Confocal 3D projections showing uninjected control WT and *s741* mutant larvae (F,H) and larvae injected with WT *furinb* messenger RNA (mRNA) (G,I). Phalloidin (purple) stained for F-actin and *Tg(Tp1:*GFP) expression (green) labeled the intrahepatic biliary cells. (J) Numbers of cysts per liver (mean ± SEM) in control and WT *furinb* mRNA-injected larvae. Each dot represents an individual liver. Statistical significance was calculated by one-way analysis of variance (ANOVA) and Tukey's *post-hoc* test: ****$p < 0.0001$. (K–M) Confocal 3D projections showing the intrahepatic bile ducts marked by *Tg(Tp1:*GFP) expression. At least five fish per genotype were examined and all showed the same phenotypes. (F–I,K–M) Ventral views; anterior is to the top. Scale bars: 70 μm (D) and 20 μm (F–I,K–M). Cys-RR, cysteine-rich region; pro, pro-domain; Sp, signal peptide; Tm, transmembrane domain.

valine to alanine amino acid change at the C-terminus of the Furinb protein (p.V822A) (Figure 3B,C). Whole-mount *in situ* hybridization revealed that *furinb* transcript is expressed in the digestive organs in zebrafish larvae (Figure 3D). Quantitative real-time PCR (PCR) showed that the *s741* mutant livers had comparable expression of *furinb* as WT at 96 hpf (Figure 3E). Injection of WT *furinb* mRNA significantly reduced the number of hepatic cysts in *s741* mutants, confirming that the missense mutation in the *furinb* gene contributes to the cystic phenotype (Figure 3F–J). To test whether Furinb is required for bile duct development, we generated *furinb* null mutants by CRISPR/Cas9 genome editing. The *furinb*^{ci204} mutant harbors a 17-bp deletion in exon 2, leading to a premature stop codon (Figure S3A). The resulting protein is predicted to truncate at the beginning of the propeptide domain (Figure S3B). *furinb*^{ci204} mutants did not show bile duct phenotypes at 96 hpf (Figure 3L). We crossed *s741* heterozygotes with *furinb*^{ci204} heterozygotes. The compound heterozygous progenies did not form hepatic cysts, but showed clustering of the biliary cells (Figure 3M), suggesting that the *s741* mutant allele is likely neomorphic.

The furinb missense mutation impairs bile duct development in a cell-autonomous manner

To determine whether the cystic phenotype seen in *s741* mutants was due to aberrant Furinb function within the biliary cells or their environment, we performed genetic mosaic analyses. We transplanted cells from the dorsolateral margin of the WT donor embryos into the blastodermal margin of the *s741* mutant host embryos at 40% epiboly and harvested the hosts at 100 hpf (Figure 4A). The WT donor cells formed bile ducts with normal appearance in the mutant host liver (Figure 4B). Conversely, when we transplanted the *s741* mutant cells into the WT host embryos, the mutant cells still formed cysts in the WT liver (Figure 4C). As a second approach, we generated *Tg(Tp1:wt-furinb-GFP)* and *Tg(Tp1:s741-furinb-GFP)* transgene constructs that drove the fusion protein expression specifically in the biliary cells. We injected the constructs into WT or *furinb*^{ci204} knockout mutants at 1–4 cell stage and examined the bile ducts at 120 hpf by Anxa4 immunostaining. The injection resulted in mosaic and transient expression of the transgene. Expression of *s741* mutant Furinb in the biliary cells promoted cystogenesis in both WT and *furinb*^{ci204} mutants (Figure 4D–K). Taken together, the mutant Furinb protein acts within the biliary cells to drive cyst formation.

The biliary cells in *s741* mutants fail to undergo proper morphogenesis to make bile ducts

To identify the morphogenic events that led to hepatic cyst formation in *s741* mutants, we performed time-course analyses by tracking the *Tg(Tp1:*GFP)+ biliary cells in WT and mutant larvae that were harvested at various time points during liver development. At 65 hpf, the biliary cells in WT and *s741* mutant livers displayed similar appearance (Figure 5A,D). At 78 hpf, the WT biliary cells interconnected to form a rudimental intrahepatic biliary network (Figure 5B). In the mutant, some cells formed connecting ducts (Figure 5E, arrows), whereas the others were clustered in isolated nodules (Figure 5E, arrowheads). The differences in the organization of biliary cells between WT and mutant were further amplified at 100 hpf (Figure 5C,F).

To characterize the cellular behaviors of biliary cells in real time, we conducted time-lapse live imaging between 80 hpf and 90 hpf. In WT (Figure 5G; Video S1), the *Tg(Tp1:*GFP)+

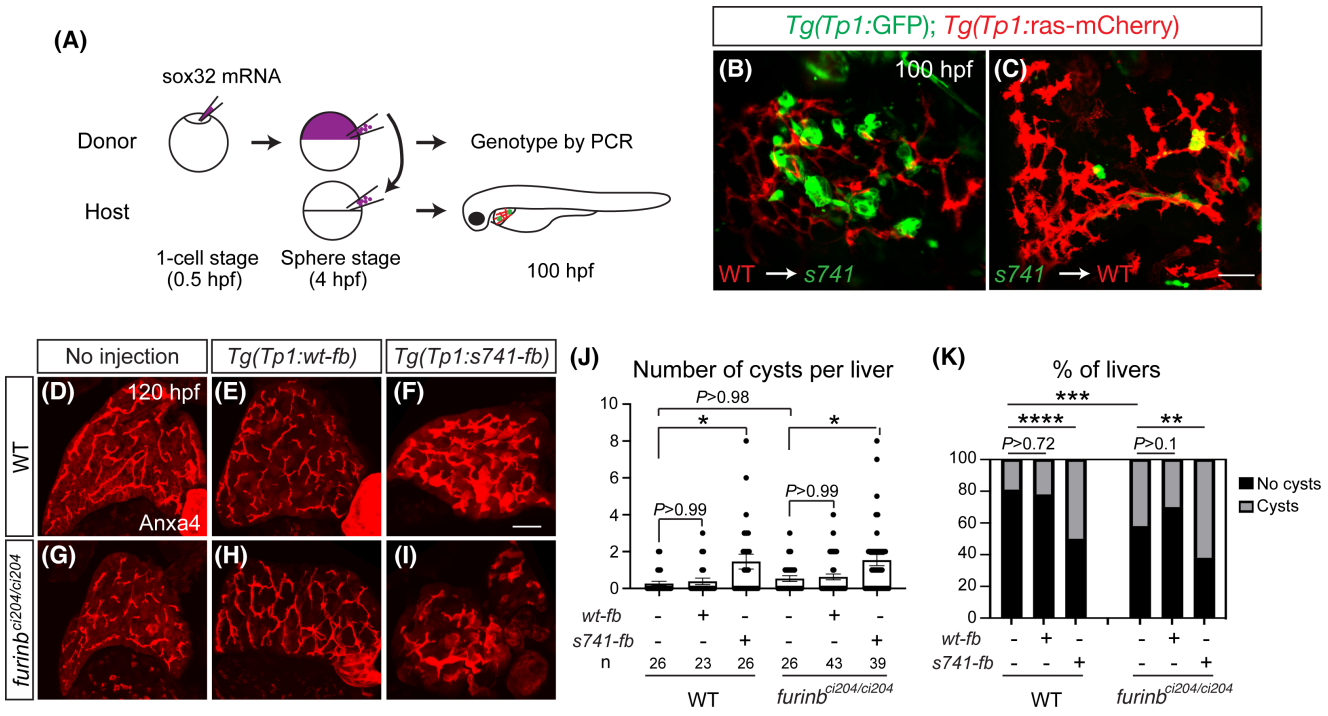

FIGURE 4 The mutant Furinb protein acts within the biliary cells to disrupt bile duct morphogenesis. (A) Schematic diagram of the genetic mosaic analysis for determining the cell autonomy of the mutant Furinb function. (B,C) Representative results of the genetic mosaic analysis. (B) WT donor cells transplanted into the *s741* mutant host liver (6 of 6 host fish exhibited the representative phenotype). (C) *s741* mutant donor cells transplanted into the WT host liver (10 of 10 host fish exhibited the representative phenotype). In both (B) and (C), the WT biliary cells expressed *Tg(Tp1:*ras-mCherry) (red) and the *s741* mutant biliary cells expressed *Tg(Tp1:*GFP) (green). (D–I) Confocal 3D projections of larvae stained with biliary marker Anxa4. Ventral view; anterior is on the top. (J,K) Numbers (mean ± SEM) of cysts per liver (J) and percentages of livers with cysts based on Anxa4 staining (K). In (J), each dot represents individual liver. Statistical significance was calculated by one-way ANOVA and Tukey's *post-hoc* test (J), and calculated by Fisher's exact test (J): *$p < 0.05$; **$p < 0.01$, ***$p < 0.001$; ****$p < 0.0001$. Scale bars: 30 μm (B,C) and 40 μm (D–I).

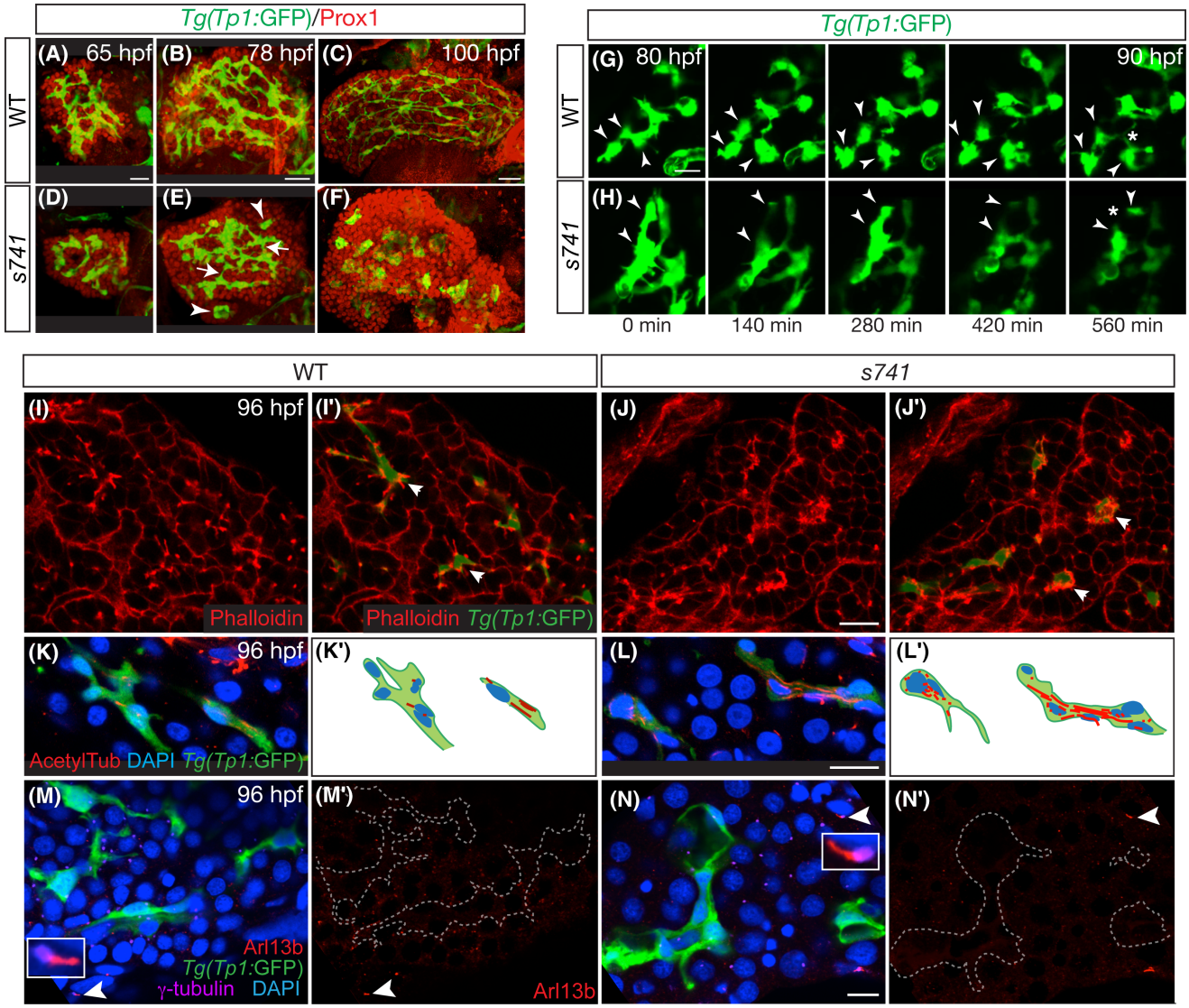

FIGURE 5 Bile duct morphogenesis was impaired in *s741* mutants. (A–F) Time-course analysis of bile duct morphogenesis. *Tg(Tp1:*GFP) expression marks the intrahepatic biliary cells (green), and Prox1 antibody labels the nuclei of hepatocytes and biliary cells (red). In (E), arrows point to the interconnecting ducts between biliary cells. Arrowheads mark biliary cell clusters that did not connect to other biliary cells. Confocal 3D projections; ventral view; anterior is on the top. Eight WT and 8 mutants were collected at each time point, and all showed the representative phenotypes. (G,H) Snapshots of time-lapse live imaging of *Tg(Tp1:*GFP)+ biliary cells in WT (n = 3) and *s741* mutants (n = 3). Arrowheads point to the same groups of biliary cells over time. Asterisk in (G) shows the new interconnecting ducts formed by the three biliary cells marked by arrowheads. Asterisk in (H) shows the loss of the pre-existing connecting duct between the two biliary cells marked by arrowheads. Confocal 3D projections; lateral view; anterior is on the left. (I,J) Larval livers stained with Phalloidin to label F-actin. (I',J') The same samples as (I) and (J) with *Tg(Tp1:*GFP) expression marking the biliary cells (green). (K,L) Larval livers stained with acetylated-tubulin/acetylTub antibody for stabilized microtubules (red), 4′,6-diamidino-2-phenylindole (DAPI) for nucleus (blue), and *Tg(Tp1:*GFP) expression for biliary cells (green). (K',L') Schematic diagrams of the biliary cells shown in (K) and (L). Nuclei and acetylated-tubulin staining are shown. (M,N) Larval livers stained with Arl13b antibody for primary cilia (red), γ-tubulin for basal bodies (purple), DAPI for nucleus (blue), and *Tg(Tp1:*GFP) expression for biliary cells (green). (M',N') The same images as in (M) and (N) but with only Arl13b staining. The biliary cells, which are outlined by dashed lines, lacked obvious Arl13b staining, whereas the neighboring cells had distinct primary cilia marked by Arl13b (white arrowheads in [M]–[N']). Inserts in (M) and (N) show high magnification images of representative primary cilia marked by arrowheads. (I–N) Confocal single plane images. Vibratome sections. Ten WT and 10 mutants were examined and all showed the representative phenotypes. Scale bars: 30 μm (A–F); 20 μm (G–J'); and 10 μm (K–N').

biliary cells were seen in clusters at the beginning of the time lapse. Over the next approximately 10 hours, individual biliary cells migrated away from each other and at the same time sent out protrusions that interconnected to form bile ducts (Figure 5G, arrowheads and asterisk[20]). In the mutant, the biliary cells showed little motility throughout the imaging time period (Video S2). Instead of extending new protrusions to make bile ducts, some cells even retracted the pre-existing connections (Figure 5H, arrowheads and asterisk), leading to nodule formation.

In mammals, hyperproliferation and apoptosis of cholangiocytes contribute to hepatic cystogenesis.[4]

To evaluate the proliferation of biliary cells, we incubated WT and mutant larvae with the replication marker 5-ethynyl-2′-deoxyuridine (EdU) from 80 hpf to 96 hpf. The percentages of biliary cells that incorporated EdU were comparable between the WT and mutant cells (Figure S4A). We only detected sporadic apoptotic cells in WT and mutant livers at 96 hpf by terminal deoxynucleotidyl transferase–mediated deoxyuridine triphosphate nick-end labeling (TUNEL) assay (Figure S4B–E). Therefore, dysregulated proliferation or apoptosis does not account for cyst formation in *s741* mutants.

Distribution of the actin and microtubule cytoskeleton is altered in *s741* mutant biliary cells

The defects in cell motility and protrusive activity prompted us to examine the actin and microtubule cytoskeleton in *s741* mutant biliary cells. Phalloidin staining showed that in WT liver, F-actin was located at the cell periphery and enriched in the bile canaliculi (Figure 5I,I'). There appeared to be an excessive accumulation of F-actin in the mutant biliary cells compared with WT (Figure 5J,J'). Immunostaining with an anti-acetylated tubulin antibody also revealed an ectopic accumulation of stabilized microtubules in the mutant biliary cells (Figure 5K–L').

In mammals, hepatic cystogenesis has been associated with defects in the primary cilium. We used an anti-ADP ribosylation factor like GTPase 13B/Arl13b antibody to specifically mark the primary cilia[24] and an anti-γ-tubulin antibody to label the basal bodies.[25] We detected primary cilia and associated basal bodies in the mesenchymal cells in WT and mutant livers (Figure 5M,N', arrowheads and inserts). However, Arl13b staining was absent in the WT and mutant biliary cells (Figure 5M,N'). Inactivation of cilia protein PC1 is responsible for ADPKD in humans.[7] We obtained zebrafish *pkd1a* single mutants and *pkd1a;pkd1b* compound mutants. Although they develop pronephric cysts at larval stages,[15] they did not form hepatic cysts (Figure S5). These results suggest that hepatic cystogenesis in *s741* mutants is not related to the impairment of primary cilia.

The *s741* missense mutation alters Furinb localization and triggers inflammation and unfolded protein response

To uncover the molecular mechanisms underlying the cystic phenotype in *s741* mutants, we performed global transcriptomic analysis on the livers of WT and *s741* mutants at 100 hpf. Gene-set enrichment analysis revealed down-regulation of metabolism pathways in the mutant livers (Figure 6A), indictive of compromised liver function. Genes involved in unfolded protein response (UPR) were up-regulated in the mutants (Figure 6B). TEM analysis also revealed dilatation of the ER lumen in the mutant hepatocytes and biliary cells, supporting the presence of ER stress (Figure 6C–F'). In *s741* mutants, the missense mutation in *furinb* leads to a valine to alanine substitution in the cytosolic domain, which is known to control the trafficking of Furin protein in mammalian cells.[26] As Furinb-specific antibody was not available, we used transgenic constructs to express either WT or *s741* mutant Furinb-GFP fusion protein in the biliary cells. We injected the constructs into WT embryos at 1–4 cell stage and performed live imaging of their livers at 120 hpf. Although the WT Furinb-GFP fusion protein was expressed along the intrahepatic bile ducts (Figure 6G), the mutant Furinb-GFP fusion protein was localized in cytoplasmic puncta within the biliary cells (Figure 6H). We generated transgenic constructs to express WT or *s741* mutant Furinb-GFP fusion protein specifically in the hepatocytes and found that the mutant protein was also mislocalized (Figure S6). Mislocalization of *s741* mutant Furinb is consistent with the increase in ER stress in these animals.

To determine whether increased ER stress contributed to the cystic phenotype, we treated the mutants and their WT and heterozygous siblings with the ER stress inhibitor 4-phenylbutyric acid (4-PBA), the ER stress inducer tunicamycin (TM), or both chemicals from 72 hpf to 120 hpf (Figure 6I). Although 4-PBA treatment did not affect bile duct morphology in WT and *s741* heterozygous larvae, TM caused clustering of the biliary cells and dilatation of the bile ducts (Figure S7). Meanwhile, inhibition of ER stress by 4-PBA significantly reduced the number of hepatic cysts in *s741* mutants. Exacerbated ER stress induced by TM increased the number of hepatic cysts in the mutants (Figure S7), and such an increase was suppressed by dual treatment with 4-PBA and TM. Therefore, ER stress contributes to cyst formation in *s741* mutants.

RNA-sequencing (RNA-seq) analysis also revealed increased inflammation in the mutant liver (Figure 6A). Consistently, we detected a more than 5-fold increase in the number of *Tg(mpeg1:*YFP)+ macrophages in the mutant livers compared with WT at 120 hpf (Figure S8A,C,F).[27] However, at 96 hpf, when the cystic phenotype first became evident in the mutants, the numbers of macrophages were comparable between WT and mutants (Figure S8E). We reason that macrophages do not contribute to the initiation of cystogenesis but may play a role in the progression of bile duct injury in the mutants.

Treatment with the mTOR inhibitor rapamycin partially rescues the cystic phenotype in *s741* mutants

To seek signaling pathways that can be targeted to suppress hepatic cystogenesis, we focused on mTOR signaling. It was up-regulated in the mutant liver as revealed

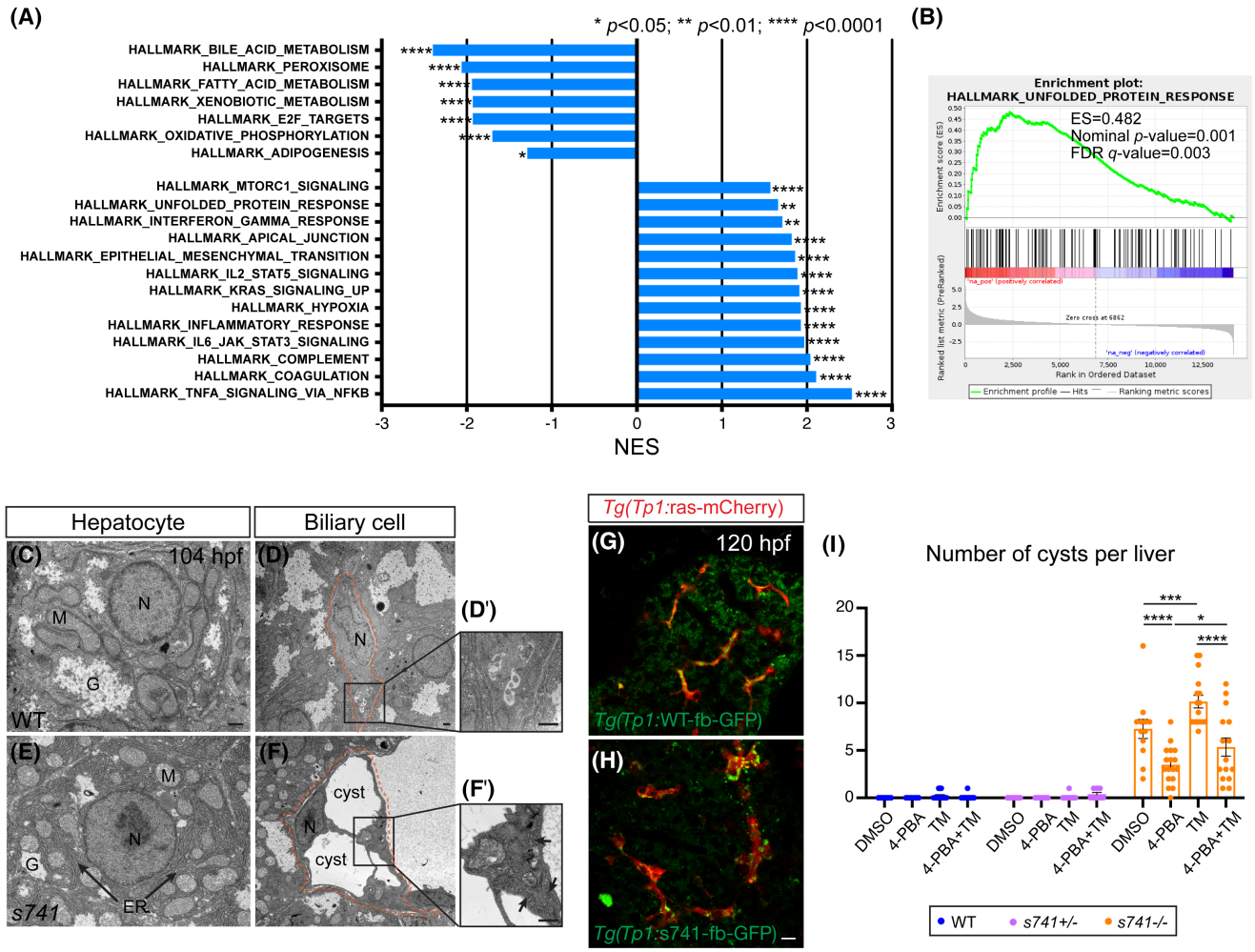

FIGURE 6 The *s741* mutation causes mislocalization of Furinb, which triggers endoplasmic reticulum (ER) stress. (A) Gene-set enrichment analysis (GSEA) identified gene sets that were significantly altered in *s741* mutant livers with nominal *p* value < 0.05 and false discovery rate (FDR) < 0.01. Gene sets were ranked by normalized enrichment score (NES). (B) GSEA plot shows a significant enrichment of unfolded protein response (UPR) pathway in *s741* mutant livers compared with WT livers. (C–F) TEM images of hepatocytes (C,E) and biliary cells (D,F). Biliary cells are outlined by orange dashed line in (D) and (F). (D') and (F') show the boxed areas in (D) and (F) under high magnification. Arrows in (E) and (F') point to dilated ER. Three WT and three mutants were examined. Scale bar: 1 μm. (G,H) Confocal single-plane images showing the expression of WT and *s741* mutant Furinb-GFP (fb-GFP) fusion proteins in the biliary cells marked by *Tg(Tp1:*ras-mCherry) expression. Sixteen WT-fb-GFP fish and 25 mut-fb-GFP fish from three rounds of injection were examined, and all had the representative protein localization. Scale bar: 10 μm. (I) Numbers (mean ± SEM) of hepatic cysts as revealed by *Tg(Tp1:*GFP) expression in the larvae after treatments with 10 μmol/L 4-4-phenylbutyric acid (4-PBA), 1 μg/mL tunicamycin (TM), or both from 72 hpf to 120 hpf. Each dot represents an individual liver. Statistical significance was calculated by one-way ANOVA and Tukey's *post-hoc* test: *$p < 0.05$; ***$p < 0.001$; ****$p < 0.0001$. ES, enrichment score; G, glycogen; M, mitochondria; N, nucleus.

by RNA-seq (Figure 7A) and has been shown to mediate both ER stress and inflammation.[28] We treated the mutants and their WT siblings with DMSO or 5 μmol/L mTOR inhibitor rapamycin from 72 hpf to 120 hpf and examined the morphology of the intrahepatic bile ducts. Rapamycin treatment did not significantly change the total number of biliary cells in WT (p = 0.9903) or *s741* mutants (p = 0.6595). Meanwhile, it reduced the number of hepatic cysts in the mutants compared with the DMSO-treated control (Figure 7B–F). Treatment with 10 μmol/L A769662, which suppresses mTOR by activating its upstream negative regulator AMP-activated protein kinase, also reduced cyst numbers in the mutants (Figure 7F). Rapamycin is a potent inducer of autophagy.[29] However, treatment with 2% trehalose, which is an mTOR-independent autophagy inducer,[30] did not decrease the number of hepatic cysts in the mutants, suggesting that rapamycin does not suppress hepatic cystogenesis by inducing autophagy. By quantitative real-time PCR, we found that the hepatic expression of UPR effector genes, including heat shock protein family A (Hsp70) member 5 *hspa5/bip*, Dnaj (Hsp40) homolog, subfamily C, member 3a (*dnajc3a*), ER degradation enhancing α-*mannosidase like protein 1* (*edem1*), and heat shock protein 90 β family member 1 (*grp94*), was significantly increased in *s741* mutants compared with WT (Figure 7G). Such increases were reversed by rapamycin treatment

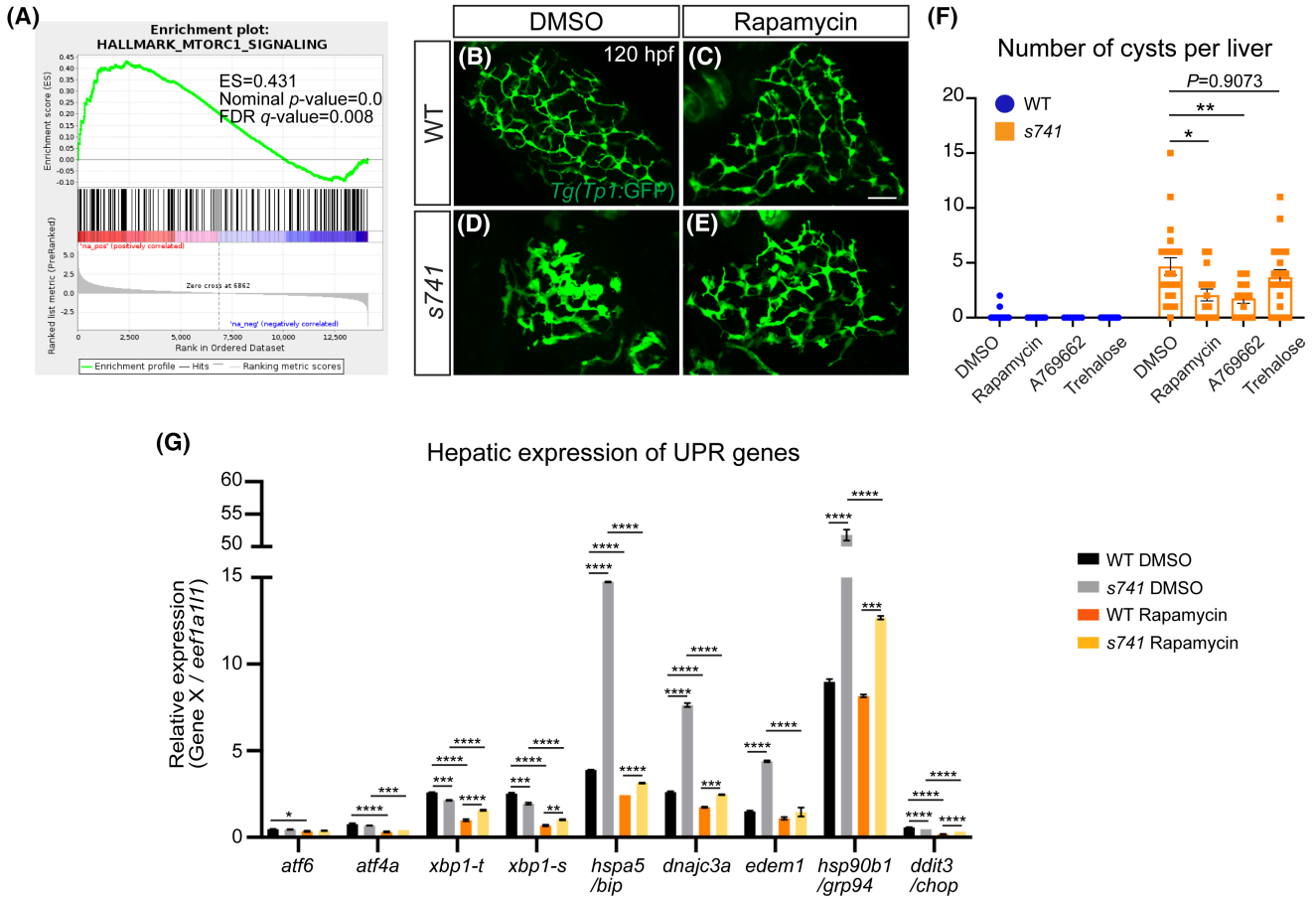

FIGURE 7 Rapamycin treatment reduces the number of hepatic cysts in *s741* mutants. (A) GSEA plot shows a significant enrichment of mammalian target of rapamycin complex 1 (mTORC1) signaling in *s741* mutant livers. (B–E) Confocal 3D projections of *Tg(Tp1:*GFP)+ biliary cells after DMSO or 5 μmol/L rapamycin treatment from 72 hpf to 120 hpf. Ventral views; anterior is on the top. Scale bar: 30 μm. (F) Numbers (mean ± SEM) of liver cysts after chemical treatments. Each point represents an individual liver. (G) Quantitative real-time PCR analyses showing the hepatic expression of UPR response genes in WT and *s741* mutants after DMSO or rapamycin treatment from 72 hpf to 120 hpf. Triplicates were performed. The results are represented as relative expression normalized to the housekeeping gene *eef1a1l1* (mean ± SEM). Statistical significance in (F) and (G) was calculated by one-way ANOVA and Tukey's *post-hoc* test: *$p < 0.05$; **$p < 0.01$; ***$p < 0.001$; ****$p < 0.0001$. *atf6*, activating transcription factor 6; *atf4a*, activating transcription factor 4a; *xbp1-t*, x-box binding protein 1-total; *xbp1-s*: x-box binding protein 1-splicing; *hspa5/bip*: heat shock protein family A (Hsp70) member 5; *dnajc3a*: Dnaj (Hsp40) homolog, subfamily C, member 3a; *edem1*: ER degradation enhancing α-mannosidase like protein 1; *hsp90b1/grp94*: heat shock protein 90 β family member 1; *ddit3/chop*: DNA damage inducible transcript 3.

(Figure 7G). Rapamycin treatment also reduced the expression of pro-inflammatory genes and the number of macrophages in the mutant livers (Figure S8B,D,F,G). Taken together, rapamycin partially suppressed hepatic cystogenesis in *s741* mutants, which coincided with the reduction in ER stress and inflammation.

DISCUSSION

Using forward genetics, we identified the first zebrafish genetic mutant that forms hepatic cysts. Hepatic cystogenesis in *s741* mutants is independent of cholangiocyte hyperproliferation or ciliopathies. Instead, changes in the actin and microtubule cytoskeleton perturb the protrusive behaviors of the biliary cells and prevent them from forming interconnecting bile ducts. We attribute the morphogenetic defects to the mislocalization of proprotein convertase Furinb caused by a missense mutation in the C-terminus and the subsequent induction of ER stress. Hepatic cystogenesis was partially suppressed by treatment with the ER stress inhibitor 4-PBA. Transcriptomic analysis revealed an increase of mammalian target of rapamycin complex 1 (mTORC1) signaling in *s741* mutants. Treatment with mTOR inhibitors ameliorated cyst formation in the mutants, at least partially by reducing ER stress.

In human and rodent, congenital hepatic cystogenesis is thought to originate from ductal plate malformation during embryogenesis.[5,6] Our study provides another example of defective bile duct development initiating hepatic cyst formation. In zebrafish, suppression of Notch signaling by injecting *jagged2/3* morpholinos resulted in cysts in the liver.[31] The cells

compromising the cysts were biliary-hepatocyte hybrid cells, reflecting defective biliary differentiation due to Notch suppression. In contrast, *s741* mutants did not have decreased Notch signaling in the liver (data not shown). The cysts in *s741* mutants were lined by biliary cells. They had reduced motility and protrusive activity and formed isolated nodules rather than interconnecting bile ducts. The impaired biliary cell behaviors were due to changes in the actin and microtubule cytoskeleton. Disorganized actin cytoskeleton has also been observed in cystic *PKD1*-null kidney epithelial cells derived from patients with ADPKD.[32] Both PC1 and PC2 interact directly with actin cytoskeleton molecules and mediate actin cytoskeleton organization and directional cell migration *in vitro*.[33–35] ARPKD human kidney tissue has excessive acetylated tubulin.[36] Treatment of microtubule-specific agents colchicine, vinblastine, and Taxol inhibits renal cyst development *in vitro*.[37] It will be interesting to investigate to what extent changes in actin and microtubules contribute to human PLDs. Disruption of actin and microtubules may also alter trafficking and localization of the channel and transporter proteins in biliary cells to enhance cyst formation.

PLDs have been linked to defects in the structure or function of primary cilia in cholangiocytes.[7] Our study suggests that ciliopathy may not cause hepatic cystogenesis in zebrafish during development. We failed to detect primary cilia in the biliary cells in larval zebrafish by immunostaining or TEM. Despite the development of renal cysts as seen in patients with ADPKD,[15] *pkd1* mutant larvae did not form liver cysts. It is noteworthy that *pkd1* mutant zebrafish are premature lethal. Whether primary cilia play a role in cholangiocyte physiology in adult zebrafish remains to be determined.

We revealed that a missense mutation in *furinb* underlies the cystic phenotypes in *s741* mutants. Furin is a proprotein convertase that functions to cleave latent precursor proteins and converts them to their active state.[26] It cycles between the trans-golgi network, cell surface, and endosomes to cleave distinct substrates depending on where it is located.[26] The mutant Furinb-GFP fusion protein is mislocalized in the biliary cells. Transforming growth factor β1, integrins, and Notch1 receptor are known FURIN substrates that also mediate bile duct development.[26,38] Our transcriptomic analyses did not detect statistically significant changes in these pathways, likely due to compensation from other proprotein convertases. However, we cannot exclude the possibility that fine-tuning of multiple pathways collectively contributes to the cystic phenotype.

We demonstrated that the mislocalized Furinb protein triggered ER stress in *s741* mutant biliary cells. In the future, we will investigate whether the mutant Furinb protein accumulates in the ER. Elevated ER stress has been observed in the liver tissue from patients with PLD and rats with polycystic kidney disease (PCK), as well as in primary cultures of human and rat cystic cholangiocytes. Chronic treatment of PCK rats with 4-PBA decreased the volumes of liver cysts.[39] It is noteworthy that the isolated PLD genes *PRKCSH*, *SEC63*, *ALG8*, *ALG9*, *SEC61B*, *GANAB*, and the ADPKD gene DnaJ heat shock protein family (Hsp40) member B11 all encode ER proteins (reviewed by Masyuk et al.[11]). It has been speculated that mutations in these genes lead to cystogenesis by affecting posttranslational modulation of PC1.[40] We propose an alternative hypothesis that mutations in the ER-associated genes may cause a broad perturbation of protein folding, maturation and trafficking, which provokes ER stress. The resulting impairment in cholangiocyte physiology and behaviors underlies cyst formation. ER stress has been connected to cytoskeleton dynamics *in vitro*. Tunicamycin treatment impaired epithelial sheet migration.[41] The ER stress sensor Inositol-requiring transmembrane kinase/endoribonuclease 1α directly interacts with filamin A and mediates cytoskeleton remodeling and cell migration.[42] Whether similar mechanisms occur in biliary cell remains to be determined.

We detected an augmentation of the mTORC1 pathway in *s741* mutants and showed that chemical inhibition of mTORC1 partially suppressed cyst formation. In patients with ADPKD and ARPKD, the epithelium lining of the hepatic cysts exhibits a markedly increase in mTOR activation.[43,44] In *Pkd2*-knockout mice, rapamycin decreases liver cystic area and cholangiocyte proliferation through inhibition of insulin-like growth factor signaling and vascular endothelial growth factor secretion.[45] We showed that rapamycin can also suppress cyst formation by reducing ER stress and inflammation,[28] but not by inducing autophagy. Evidence from different pathological conditions has shown that mTORC1 operates both upstream and downstream of UPR signals, which can either enhance or antagonize the anabolic function of mTORC1.[46] The bidirectional crosstalk between ER stress and mTOR likely exists in biliary cells during cystogenesis. Clinical trials testing the efficacy of mTOR inhibitor treatment in PKD yielded conflicting results.[11] Our results shed light on the mechanisms underlying rapamycin's action on cystogenesis and reveal additional therapeutic targets to improve treatment.

Our study provides an excellent example of how forward genetic screen elucidates biological phenomena that cannot be captured by knockout animals. *Furin*-null mice die between E10.5-E11.5 due to heart malformation and failure of axial rotation.[47] *furinb* knockout zebrafish and liver-specific knockout of Furin in mice[48,49] do not cause obvious liver injury. The *s741* mutation is a neomorphic allele that only causes cysts in the homozygous mutant or when it is overexpressed in WT by transgene. Given that mutations in the known disease genes only account for 50% of clinical cases of PLD,[4] forward genetic screen in model organisms remains a

powerful tool to discover genes and mechanisms for hepatic cystogenesis.

ACKNOWLEDGMENT

The authors thank Dr. Matthew Kofron at CCHMC Confocal Imaging Core for assistance with confocal imaging and post analyses, Drs. Stacey Huppert and Jorge Bezerra for discussions, Drs Adam Miller, Breanne Harty, and Kelly Monk for technical advice on whole genome sequencing, Dr. Zhaoxia Sun for the Arl13b antibody, Drs Jacek Topczewski and Lindsey Barske for examining the mutant jaw phenotypes, Ms. Jessica Webster at the CCHMC EM core for assistance with TEM, and Mr. Bryan Donnelly for advice on biochemical assays. They also acknowledge CCHMC Veterinary Services for fish care, and Ryan Stefancik, Allison Ross, Zenab Saeed, and Hannah Nartker for research assistance.

FUNDING INFORMATION

Supported by National Institutes of Health (NIH) (R00 AA020514, R01 DK117266-01A1, and P30 DK078392); a Trustee Award from the Cincinnati Children's Research Foundation; the Peter and Tommy Colucci Research Award for PFIC from the Center for Undiagnosed and Rare Liver Disease at Cincinnati Children's Research Foundation; a Pilot/Feasibility grant from the University of California, San Francisco Liver Center; NIH/National Cancer Institute (K08 CA172288 and R01 CA222570); Damon Runyon Cancer Research Foundation (DRG-109-10); and an Arnold W. Strauss Fellow Award.

CONFLICT OF INTEREST

Nothing to report.

ORCID

Chunyue Yin https://orcid.org/0000-0002-3784-6363

REFERENCES

1. Rawla P, Sunkara T, Muralidharan P, Raj JP. An updated review of cystic hepatic lesions. Clin Exp Hepatol. 2019;5:22–9.
2. Drenth JP, Chrispijn M, Nagorney DM, Kamath PS, Torres VE. Medical and surgical treatment options for polycystic liver disease. Hepatology. 2010;52:2223–30.
3. Larusso NF, Masyuk TV, Hogan MC. Polycystic liver disease: the benefits of targeting cAMP. Clin Gastroenterol Hepatol. 2016;14:1031–4.
4. Fabris L, Fiorotto R, Spirli C, Cadamuro M, Mariotti V, Perugorria MJ, et al. Pathobiology of inherited biliary diseases: a roadmap to understand acquired liver diseases. Nat Rev Gastroenterol Hepatol. 2019;16:497–511.
5. Beaudry JB, Cordi S, Demarez C, Lepreux S, Pierreux CE, Lemaigre FP. Proliferation-independent initiation of biliary cysts in polycystic liver diseases. PLoS One. 2015;10:e0132295.
6. Raynaud P, Tate J, Callens C, Cordi S, Vandersmissen P, Carpentier R, et al. A classification of ductal plate malformations based on distinct pathogenic mechanisms of biliary dysmorphogenesis. Hepatology. 2011;53:1959–66.
7. Mansini AP, Peixoto E, Thelen KM, Gaspari C, Jin S, Gradilone SA. The cholangiocyte primary cilium in health and disease. Biochim Biophys Acta Mol Basis Dis. 2018;1864:1245–53.
8. Hughes J, Ward CJ, Peral B, Aspinwall R, Clark K, San Millan JL, et al. The polycystic kidney disease 1 (PKD1) gene encodes a novel protein with multiple cell recognition domains. Nat Genet. 1995;10:151–60.
9. Mochizuki T, Wu G, Hayashi T, Xenophontos SL, Veldhuisen B, Saris JJ, et al. PKD2, a gene for polycystic kidney disease that encodes an integral membrane protein. Science. 1996;272:1339–42.
10. Zhang MZ, Mai W, Li C, Cho SY, Hao C, Moeckel G, et al. PKHD1 protein encoded by the gene for autosomal recessive polycystic kidney disease associates with basal bodies and primary cilia in renal epithelial cells. Proc Natl Acad Sci U S A. 2004;101:2311–6.
11. Masyuk TV, Masyuk AI, LaRusso NF. Polycystic liver disease: advances in understanding and treatment. Annu Rev Pathol. 2022;17:251–69.
12. Pham DH, Yin C. Zebrafish as a model to study cholestatic liver diseases. Methods Mol Biol. 2019;1981:273–89.
13. Tietz Bogert PS, Huang BQ, Gradilone SA, Masyuk TV, Moulder GL, Ekker SC, et al. The zebrafish as a model to study polycystic liver disease. Zebrafish. 2013;10:211–7.
14. Monk KR, Voas MG, Franzini-Armstrong C, Hakkinen IS, Talbot WS. Mutation of sec63 in zebrafish causes defects in myelinated axons and liver pathology. Dis Model Mech. 2013;6:135–45.
15. Zhu P, Sieben CJ, Xu X, Harris PC, Lin X. Autophagy activators suppress cystogenesis in an autosomal dominant polycystic kidney disease model. Hum Mol Genet. 2017;26:158–72.
16. Ninov N, Borius M, Stainier DY. Different levels of Notch signaling regulate quiescence, renewal and differentiation in pancreatic endocrine progenitors. Development. 2012;139:1557–67.
17. Leshchiner I, Alexa K, Kelsey P, Adzhubei I, Austin-Tse CA, Cooney JD, et al. Mutation mapping and identification by whole-genome sequencing. Genome Res. 2012;22:1541–8.
18. Chung WS, Stainier DY. Intra-endodermal interactions are required for pancreatic beta cell induction. Dev Cell. 2008;14:582–93.
19. Kwan KM, Fujimoto E, Grabher C, Mangum BD, Hardy ME, Campbell DS, et al. The Tol2kit: a multisite gateway-based construction kit for Tol2 transposon transgenesis constructs. Dev Dyn. 2007;236:3088–99.
20. Lorent K, Moore JC, Siekmann AF, Lawson N, Pack M. Reiterative use of the notch signal during zebrafish intrahepatic biliary development. Dev Dyn. 2010;239:855–64.
21. Parsons MJ, Pisharath H, Yusuff S, Moore JC, Siekmann AF, Lawson N, et al. Notch-responsive cells initiate the secondary transition in larval zebrafish pancreas. Mech Dev. 2009;126:898–912.
22. Otis JP, Farber SA. Imaging vertebrate digestive function and lipid metabolism. Drug Discov Today Dis Models. 2013;10:e11–6.
23. Walker MB, Miller CT, Coffin Talbot J, Stock DW, Kimmel CB. Zebrafish furin mutants reveal intricacies in regulating Endothelin1 signaling in craniofacial patterning. Dev Biol. 2006;295:194–205.
24. Duldulao NA, Lee S, Sun Z. Cilia localization is essential for in vivo functions of the Joubert syndrome protein Arl13b/Scorpion. Development. 2009;136:4033–42.
25. Lunt SC, Haynes T, Perkins BD. Zebrafish ift57, ift88, and ift172 intraflagellar transport mutants disrupt cilia but do not affect hedgehog signaling. Dev Dyn. 2009;238:1744–59.
26. Thomas G. Furin at the cutting edge: from protein traffic to embryogenesis and disease. Nat Rev Mol Cell Biol. 2002;3:753–66.

27. Roca FJ, Ramakrishnan L. TNF dually mediates resistance and susceptibility to mycobacteria via mitochondrial reactive oxygen species. Cell. 2013;153:521–34.
28. Saxton RA, Sabatini DM. mTOR signaling in growth, metabolism, and disease. Cell. 2017;169:361–71.
29. Noda T, Ohsumi Y. Tor, a phosphatidylinositol kinase homologue, controls autophagy in yeast. J Biol Chem. 1998;273:3963–6.
30. Mardones P, Rubinsztein DC, Hetz C. Mystery solved: trehalose kickstarts autophagy by blocking glucose transport. Sci Signal. 2016;9:fs2.
31. Lorent K, Yeo SY, Oda T, Chandrasekharappa S, Chitnis A, Matthews RP, et al. Inhibition of jagged-mediated Notch signaling disrupts zebrafish biliary development and generates multi-organ defects compatible with an Alagille syndrome phenocopy. Development. 2004;131:5753–66.
32. Streets AJ, Prosseda PP, Ong AC. Polycystin-1 regulates ARHGAP35-dependent centrosomal RhoA activation and ROCK signaling. JCI Insight. 2020;5:e135385.
33. Boca M, D'Amato L, Distefano G, Polishchuk RS, Germino GG, Boletta A. Polycystin-1 induces cell migration by regulating phosphatidylinositol 3-kinase-dependent cytoskeletal rearrangements and GSK3beta-dependent cell cell mechanical adhesion. Mol Biol Cell. 2007;18:4050–61.
34. Gallagher AR, Cedzich A, Gretz N, Somlo S, Witzgall R. The polycystic kidney disease protein PKD2 interacts with Hax-1, a protein associated with the actin cytoskeleton. Proc Natl Acad Sci U S A. 2000;97:4017–22.
35. Yao G, Su X, Nguyen V, Roberts K, Li X, Takakura A, et al. Polycystin-1 regulates actin cytoskeleton organization and directional cell migration through a novel PC1-Pacsin 2-N-Wasp complex. Hum Mol Genet. 2014;23:2769–79.
36. Berbari NF, Sharma N, Malarkey EB, Pieczynski JN, Boddu R, Gaertig J, et al. Microtubule modifications and stability are altered by cilia perturbation and in cystic kidney disease. Cytoskeleton (Hoboken). 2013;70:24–31.
37. Woo DD, Miao SY, Pelayo JC, Woolf AS. Taxol inhibits progression of congenital polycystic kidney disease. Nature. 1994;368:750–3.
38. Zong Y, Stanger BZ. Molecular mechanisms of liver and bile duct development. Wiley Interdiscip Rev Dev Biol. 2012;1:643–55.
39. Santos-Laso A, Izquierdo-Sanchez L, Rodrigues PM, Huang BQ, Azkargorta M, Lapitz A, et al. Proteostasis disturbances and endoplasmic reticulum stress contribute to polycystic liver disease: new therapeutic targets. Liver Int. 2020;40:1670–85.
40. Besse W, Dong K, Choi J, Punia S, Fedeles SV, Choi M, et al. Isolated polycystic liver disease genes define effectors of polycystin-1 function. J Clin Invest. 2017;127:3558.
41. Gipson IK, Kiorpes TC, Brennan SJ. Epithelial sheet movement: effects of tunicamycin on migration and glycoprotein synthesis. Dev Biol. 1984;101:212–20.
42. Urra H, Henriquez DR, Canovas J, Villarroel-Campos D, Carreras-Sureda A, Pulgar E, et al. IRE1alpha governs cytoskeleton remodelling and cell migration through a direct interaction with filamin A. Nat Cell Biol. 2018;20:942–53.
43. Becker JU, Opazo Saez A, Zerres K, Witzke O, Hoyer PF, Schmid KW, et al. The mTOR pathway is activated in human autosomal-recessive polycystic kidney disease. Kidney Blood Press Res. 2010;33:129–38.
44. Qian Q, Du H, King BF, Kumar S, Dean PG, Cosio FG, et al. Sirolimus reduces polycystic liver volume in ADPKD patients. J Am Soc Nephrol. 2008;19:631–8.
45. Spirli C, Okolicsanyi S, Fiorotto R, Fabris L, Cadamuro M, Lecchi S, et al. Mammalian target of rapamycin regulates vascular endothelial growth factor-dependent liver cyst growth in polycystin-2-defective mice. Hepatology. 2010;51:1778–88.
46. Appenzeller-Herzog C, Hall MN. Bidirectional crosstalk between endoplasmic reticulum stress and mTOR signaling. Trends Cell Biol. 2012;22:274–82.
47. Roebroek AJ, Umans L, Pauli IG, Robertson EJ, van Leuven F, Van de Ven WJ, et al. Failure of ventral closure and axial rotation in embryos lacking the proprotein convertase Furin. Development. 1998;125:4863–76.
48. Roebroek AJ, Taylor NA, Louagie E, Pauli I, Smeijers L, Snellinx A, et al. Limited redundancy of the proprotein convertase furin in mouse liver. J Biol Chem. 2004;279:53442–50.
49. Essalmani R, Susan-Resiga D, Chamberland A, Abifadel M, Creemers JW, Boileau C, et al. In vivo evidence that furin from hepatocytes inactivates PCSK9. J Biol Chem. 2011;286:4257–63.
50. Zhang D, Golubkov VS, Han W, Correa RG, Zhou Y, Lee S, et al. Identification of Annexin A4 as a hepatopancreas factor involved in liver cell survival. Dev Biol. 2014;395:96–110.

SUPPORTING INFORMATION

Additional supporting information can be found online in the Supporting Information section at the end of this article.

How to cite this article: Ellis JL, Evason KJ, Zhang C, Fourman MN, Liu J, Ninov N, et al. A missense mutation in the proprotein convertase gene *furinb* causes hepatic cystogenesis during liver development in zebrafish. Hepatol Commun. 2022;6:3083–3097. https://doi.org/10.1002/hep4.2038